

# Cooperative Spectrum Detection System with Multicarrier BPSK Transmitters and Double-Sampling Rate DMC Receiver

Ali Alqatawneh\*

Department of Communication and Computer Engineering, Tafila Technical University, Tafila, Jordan  
E-mail: ali.katawneh74@gmail.com

Received: October 15, 2019

Revised: November 9, 2019

Accepted: November 16, 2019

**Abstract**— The employment of a double-sampling rate (DSR) at the receiver of the decision-making center (DMC) in a multicarrier cooperative spectrum detection (CSD) system is investigated in this paper. The spectrum detection is obtained for a cognitive mobile communication network with a single licensed user (LU) and multiple cognitive users (CUs). In the investigated system, each CU performs a local-detection independently; based on the local detection, a single-bit local-decision is taken at each CU. Decisions from CUs are modulated using a binary phase-shift keying (BPSK) and then transmitted to the DMC over orthogonal subcarriers and under frequency-selective Rayleigh fading channels. Signals from CUs are observed at the DMC receiver and sampled at a rate twice that of the transmitter to gain diversity. The results - verified using Matlab plots - show that using the DSR at the DMC receiver reduces the overall sensing errors and removes performance degradation effects due to the timing-offset between the CUs transmitters and the DMC receiver. Moreover, these improvements are achieved without any degradation in the spectral-efficiency of the system or increase in the complexity of the transmitter at the CU.

**Keywords**— Cognitive radio; spectrum sensing; false-alarm; miss-detection; Double-sampling rate; Decision-making center.

## 1. INTRODUCTION

Cognitive radio is a frequency spectrum sharing and allocating technology [1]; this technology can be used to tackle the challenge of the radio spectrum shortage. The spectrum shortage comes from the low utilization efficiency of the allocated frequency bands, the rising worldwide demand for mobile wireless multimedia communication, and the accelerated growth of mobile communication users. In a cognitive mobile communication (CMC) network, it is necessary to distinguish between two kinds of mobile users: a cognitive user (CU) and a licensed user (LU). The priority for using the licensed-spectrum is for the LU; however, the CU can utilize the licensed-spectrum when it is not being used by the LU [2]. In the CMC network, a licensed-spectrum detection process is periodically performed to explore and define the unutilized frequency bands in the licensed frequency spectrum. These bands must be detected correctly and quickly to maximize the opportunities for using these bands by the CU. Besides, accurate empty bands detection can significantly reduce the interference opportunities between CUs and LU in the CMC network.

For the detection of an unutilized licensed-spectrum, energy detectors are commonly employed because of their low computing complication and their simple hardware implementation. Also, the operation of these detectors does not need any previous information about the LU signal. However, the major drawback of energy detectors is their low performance at a very low received signal-to-noise ratio (SNR)

\* Corresponding author

[2, 3]. Due to channel imperfections such as noise and fading, independent signal detection by each CU might not be authentic enough to make a correct decision about whether the detected frequency band is empty or occupied by the LU signal. Failing to detect the correct occupation status of the licensed-spectrum can result in interference between the LU and CU or lead the CU to miss an opportunity to utilize the empty licensed-spectrum. Therefore, to reduce the errors of LU signal detection, many cooperative spectrum detection (CSD) schemes have been suggested; the provided spatial diversity in cooperative spectrum sensing can significantly improve the spectrum detection performance [3, 4]. In general, the CSD system involves three consecutive stages: local-spectrum detection, local-decision reporting, and final-decision making. In the first stage, each CU performs an independent local-detection for the LU signal in the licensed-band. Based on the local-detection, a local-decision (whether the spectrum is occupied or not) is taken by the CU. In the second stage, each CU forwards either the observed energy value or a one-bit local-decision to a decision-making center (DMC). At the DMC, the overall-final decision (whether the licensed-spectrum is occupied or empty) is taken according to a specific decision-rule to meet predefined performance conditions [4]. For brevity, the channel between the LU and the CU and the channel between the CU and the DMC are referred to as the sensing-channel and the reporting-channel, respectively.

The noise-free reporting-channel assumption in the CSD system is not reasonable in practical systems; this assumption might lead to spectrum detection errors [5]. However, CSD over an imperfect reporting-channel can reflect a better representation of realistic channel conditions [6, 7]. In [6, 7], the CU local-decision is transmitted to a DMC over a reporting-channel corrupted by noise. Authors in [8] consider a CSD scheme for a Wi-Fi network, where the reporting-channel experiences flat fading. In [9], an optimal final decision rule for hard combining is derived for CSD system with a composite fading reporting-channel. The mixture of Gaussian-distribution is used to model the statistics of the composite fading reporting-channel [9].

A CSD system, where the detection and the reporting tasks take place over noisy and flat Rayleigh-fading channels, is shown in [10]. In [10], the period for the LU signal detection is assumed to be much shorter than the average of the LU state transition period. Furthermore, exact channel statistics for the sensing-channel and the reporting-channel is considered in the system design. In [11-13], authors consider CSD systems with approximate channel statistics, exact channel state information (CSI), and an estimated instantaneous CSI, respectively. In [14], the performance of the CSD system is investigated, where the sensing-channels are corrupted by noise and Log-normal shadowing (LNS). However, the reporting-channels in [14] are assumed to be noise-free. A CSD system with energy detectors over  $\alpha$ - $\kappa$ - $\mu$  fading sensing-channels is presented in [15], where the exact closed-form for detection probability is derived. Also, in [15], the maximum-ratio combining (MRC) diversity, the square-law combining (SLC) diversity, and the square-law selection (SLS) diversity are investigated at the central receiver of the CSD system. However, the sensing-channel in [15] is considered as a noise-free channel, which is not an accurate for realistic mobile and wireless networks.

An orthogonal frequency division multiplexing (OFDM) is adopted in [16] to report one-bit local decisions from cognitive radio users to a final-decision center over multipath fading channels. Also, the author in [16] shows that with or without perfect knowledge of the CSI at the decision center, the soft-decisions fusion outperforms the hard-decisions fusion. However, the soft-decisions fusion is optimum if the receiver of the decision center has a perfect knowledge of the CSI. In [17, 18], authors show that the symbol error rate of multicarrier modulation can be significantly improved using time-domain oversampling at the receiver. The performance improvement comes from the multipath diversity enhancement introduced by the oversampling. In addition, the multicarrier systems with time-domain oversampling can achieve performance improvements without any reduction in systems spectral efficiency. Results in [18] show that the time-domain oversampling at the receiver can effectively illuminate spectrum aliasing and remove the negative-impact of the timing-offset between the transmission and receiving units.

In this paper, a CSD system that employs multicarrier orthogonal signals to report one-bit local-decisions from CUs to a DMC over frequency-selective Rayleigh fading channels is introduced and the effect of using the DSR at the DMC receiver on the overall performance of the system-assessed using the overall miss-detection probability, overall false-alarm probability, and overall sensing error probability-is investigated using Matlab plots.

Throughout the paper, the following notations are used:  $\mathbf{I}_M$  denotes  $M \times M$  identity matrix;  $\mathbf{I}^{(k)}_M$  is the  $k$ -th column of the identity matrix  $\mathbf{I}_M$ ;  $E[\cdot]$  denotes the mathematical expectation;  $(\cdot)^H$  denotes the Hermitian operation;  $\otimes$  denotes the Kronecker product; and  $\mathbb{C}$  denotes the complex space. Also, Matrices and column vectors are denoted by uppercase boldface and lowercase boldface, respectively.

## 2. CSD SYSTEM MODEL

Consider a CSD system with one LU,  $K$  CUs, and a single DMC, where the final-decision whether the licensed band is occupied or empty is made. The CSD process consists of three consecutive stages: the local spectrum detection, decision reporting, and final decision-making. In the local spectrum-detection, each CU carries out a local spectrum detection individually using an energy detector. Based on the local spectrum detection, each CU takes a binary decision, whether the frequency band is empty or occupied by the LU signal. In the reporting stage, each CU forwards its local-decision to a DMC over quasi-static frequency-selective Rayleigh fading channels corrupted by noise. Third, based on the observed local-decisions at DMC, the final decision (whether the explored licensed-spectrum is empty or occupied) is taken according to a decision rule. For simplicity purposes, the proposed system presumes that all CUs in the CSD system utilize the same types of energy detectors; and they are close to each other such that they observe almost the same energy from the LU. During the local spectrum detection, the received LU energy signal at the  $k$ -th CU can be expressed as [6]:

$$\chi_k(t) = \begin{cases} p(t) + n_k(t), & \text{occupied spectrum} \\ n_k(t), & \text{emptyspectrum,} \end{cases} \quad (1)$$

where  $\chi_k(t)$ ,  $p(t)$ , and  $n_k(t)$  denote the signal observed by the  $k$ -th CU, the LU transmitted signal, and the additive white Gaussian noise with variance  $N_o$ , respectively. Based on Eq. (1), the local-decision at each CU can be expressed as [6]:

$$d = \begin{cases} 1, & \text{occupied licensed-spectrum} \\ 0, & \text{empty licensed-spectrum} \end{cases} \quad (2)$$

The performance of the CSD system can be defined based on the following error metrics: the false-alarm where the CU claims that the licensed-spectrum is being used by the LU when the LU is inactive, and the miss-detection where the CU claims that the licensed-spectrum is empty when the LU is active [6]. Based on Eqs. (1-3), the local false-alarm and the local miss-detection probabilities for the  $k$ -th CU can be evaluated respectively as [9]:

$$P_{f_k} = \frac{\Gamma(\mu_k, \lambda/2)}{\Gamma(\mu_k)} \quad (3)$$

$$P_{m_k} = 1 - Q_{\mu_k}(\sqrt{2\gamma_s}, \sqrt{\lambda}) \quad (4)$$

where  $\lambda$  denotes the energy-threshold of the energy detector at the CUs which is determined to meet certain probabilities of false-alarm and miss-detection;  $\Gamma(\mu_k)$  stands for the Gamma function;  $\Gamma(\mu_k, \lambda/2)$  is the incomplete Gamma function with  $\mu_k$  being the signal time-bandwidth product of the  $k$ -th CU;  $Q_{\mu_k}(\sqrt{2\gamma_s}, \sqrt{\lambda})$  denotes the Generalized Marcum Q function; and  $\gamma_s = E_p/N_o$  with  $E_p$  is the LU average transmitted energy. The local decisions are mapped to BPSK symbols and transmitted to the DMC using orthogonal subcarriers over imperfect reporting-channels. The baseband representation of the mapped signal can be expressed as [6]:

$$s = (2d - 1) = \begin{cases} 1, & \text{occupied spectrum} \\ -1, & \text{empty spectrum} \end{cases} \quad (5)$$

For the  $k$ -th CU, the false-alarm and miss-detection probabilities at the DMC can be described respectively as [8]:

$$\tilde{P}_{f_k} = P_{f_k}(1 - e_k) + e_k(1 - P_{f_k}) \quad (6)$$

$$\tilde{P}_{m_k} = P_{m_k}(1 - e_k) + e_k(1 - P_{m_k}) \quad (7)$$

where  $\tilde{P}_{f_k}$ ,  $\tilde{P}_{m_k}$ , and  $e_k$  are the false-alarm probability of the  $k$ -th CU at the DMC, the miss-detection probability of the  $k$ -th CU at the DMC, and the error probability of sending the local-decision from the  $k$ -th CU to the DMC, respectively.

The optimum receiver at the DMC, the error performance of the reporting-channel, and the overall decision at the DMC are presented in the following three subsections, respectively.

## 2.1. DMC Optimum Receiver Analysis

The local decision-symbols from  $K$  CUs are transmitted to the DMC over orthogonal subcarriers by using an inverse discrete Fourier transform (IDFT). The

fundamental frequency of the modulated subcarrier is  $f_o = 1/T_o$ , where  $T_o$  is the fundamental period subcarrier. The produced time-domain signal is then sampled at a sampling period of  $T_1 = T_o/K$ , which produces  $K$  time-domain samples. Acyclic prefix is added to time-domain samples before transmission to the DMC. The sum of the time-domain samples from  $K$  CUs is first observed by the DMC receiver and then passed through a filter. The output of the filter is double-sampled with a sampling period of  $T_2 = T_1/2$  followed by removing the cyclic prefix. If the transmitted base-band symbol from the  $k$ -th CU is  $s_k \in \{-1,1\}$ , then based on [18], the time-domain representation of the signals sum from CUs observed at the DMC can be written in a matrix representation as:

$$\mathbf{y} = \sqrt{E_s} \sum_{k=1}^K \mathbf{H}_k (\mathbf{Q}_K^H \mathbf{s}_k) + \mathbf{w} = \sqrt{E_s} \sum_{k=1}^K \mathbf{H}_k \mathbf{x}_k + \mathbf{w} \quad (8)$$

where  $\mathbf{y} \in C^{2K \times 1}$  is the observed signals-sum at the DMC;  $E_s$  is the average transmitted energy per transmitted symbol;  $\mathbf{H}_k \in C^{2K \times K}$  is the time-domain channel matrix [17];  $\mathbf{Q}_K \in C^{K \times K}$  is the discrete Fourier transform (DFT) matrix of size  $K$ ,  $\mathbf{x}_k = \mathbf{Q}_K^H \mathbf{s}_k = [x(0), \dots, x(K-1)]^H \in C^{K \times 1}$  is the time-domain transmitted samples from the  $k$ -th CU toward the DMC with  $\mathbf{s}_k = (\mathbf{I}_K)^k s_k \in C^{K \times 1}$ ; and  $\mathbf{w} = [w(0), \dots, w(2K-1)]^H \in C^{2K \times 1}$  is the noise vector with covariance matrix  $\mathbf{R}^w = E[\mathbf{w}\mathbf{w}^H] \in C^{2K \times 2K}$ . The time-domain channel matrix  $\mathbf{H}_k$  can be written as [18]:

$$\mathbf{H}_k = \begin{bmatrix} h_k(0) & 0 & \dots & h_k(\tilde{L}) & \dots & h_k(1) \\ h_k(1) & h_k(0) & \dots & 0 & h_k(\tilde{L}) & \dots \\ \vdots & \ddots & \ddots & \ddots & \ddots & \vdots \\ 0 & \dots & h_k(\tilde{L}) & \dots & \dots & h_k(0) \end{bmatrix} \quad (9)$$

where  $\tilde{L} = 2L-1$  with  $L$  is the length of the time-domain complex channel coefficients vector related to the  $k$ -th CU; and  $\mathbf{h}_k = [h_k(0), h_k(1), \dots, h_k(\tilde{L})]^T \in C^{\tilde{L} \times 1}$  is the complex channel coefficients associated with the  $k$ -th CU with a covariance matrix given as  $\mathbf{R}_k^h = E[\mathbf{h}_k \mathbf{h}_k^H] \in C^{\tilde{L} \times \tilde{L}}$ . The frequency-domain representation of Eq. (8) can be attained by multiplying Eq. (8) with DFT channel matrix of size  $2K$  [18]. The result of multiplication can be expressed as:

$$\mathbf{r} = \sqrt{E_s} \sum_{k=1}^K \mathbf{G}_k \mathbf{I}_K^{(k)} s_k + \mathbf{z} = \sqrt{E_s} \sum_{k=1}^K \mathbf{g}_k s_k + \mathbf{z} \quad (10)$$

where  $\mathbf{r} = \mathbf{Q}_{2K} \mathbf{y} \in C^{2K \times 1}$ ,  $\mathbf{Q}_{2K} \in C^{2K \times 2K}$  is the DTF matrix of size  $2K$ ;  $\mathbf{z} = \mathbf{Q}_{2K} \mathbf{w} \in C^{2K \times 1}$  is the frequency domain noise vector with covariance matrix  $\mathbf{R}^z = \mathbf{Q}_{2K} \mathbf{R}^w \mathbf{Q}_{2K}^H \in C^{2K \times 2K}$ ,  $\mathbf{G}_k = \mathbf{Q}_{2K} \mathbf{H}_k \mathbf{Q}_K \in C^{2K \times K}$  is the frequency-domain channel matrix; and  $\mathbf{g}_k = \mathbf{G}_k \mathbf{I}_K^{(k)} \in C^{2K \times 1}$  is the  $k$ -th column of the matrix  $\mathbf{G}_k$ . It should

be noted that the computational complexity of calculating the frequency domain channel matrix  $\mathbf{G}_k$  is  $o(6K^3)$  for CSD system with DSR DMC receiver while the computational complexity of  $\mathbf{G}_k$  is  $o(2K^3)$  for system with  $T_2 = T_1$ .

The frequency-domain channel coefficients matrix  $\mathbf{G}_k$  can be rewritten as [18]:

$$\mathbf{G}_k = \begin{bmatrix} \mathbf{G}_k^0 & \mathbf{G}_k^1 \end{bmatrix}^T \tag{11}$$

where  $\mathbf{G}_k^0 \in C^{K \times K}$  and  $\mathbf{G}_k^1 \in C^{K \times K}$ . Because of the diagonal structure of both  $\mathbf{G}_k^0$  and  $\mathbf{G}_k^1$ , all elements of the vector  $\mathbf{g}_k$  are zeros except the  $k$ -th and the  $(k+N)$ -th elements [18]. Thus the received signal associated with the symbol transmitted from the  $k$ -th CU can be described by:

$$\mathbf{r}_k = \sqrt{E_s} \hat{\mathbf{g}}_k \cdot s_k + \mathbf{z}_k \tag{12}$$

where  $\mathbf{r}_k = [r(k), r(k+N)]^T \in C^{2 \times 1}$  is the observed frequency-domain signal at the DMC from the  $k$ -th CU,  $\hat{\mathbf{g}}_k = [g_k(k), g_k(k+K)]^H \in C^{2 \times 1}$  is the frequency-domain channel vector related to the  $k$ -th CU; and  $\mathbf{z}_k = [n(k), n(k+K)]^H \in C^{2 \times 1}$  is the noise vector associated with the  $k$ -th CU. The system in Eq. (12) provides multiple outputs for the same input symbol; thus, the maximum ratio combining (MRC) can be adopted at the DMC receiver to harvest the maximum diversity gain. However, the noise vector in Eq. (12) consists of correlated noise elements; and the noise is no longer a white noise. Thus, before using the MRC in Eq. (12), the system should be converted to an equivalent system with uncorrelated noise elements.

*Proposition:* A system with correlated noise-samples as in Eq. (12) can be represented by an equivalent system with uncorrelated noise samples as:

$$\tilde{\mathbf{r}}_k = \sqrt{E_s} \tilde{\mathbf{g}}_k \cdot s_k + \tilde{\mathbf{z}}_k \tag{13}$$

where  $\tilde{\mathbf{r}}_k = \mathbf{D}_k \mathbf{r}_k$ ,  $\tilde{\mathbf{g}}_k = \mathbf{D}_k \hat{\mathbf{g}}_k$ , and  $\tilde{\mathbf{z}}_k = \mathbf{D}_k \mathbf{z}_k$  with  $\mathbf{D}_k = \sqrt{N_0} (\mathbf{R}_k^z)^{-\frac{1}{2}}$  is the decorrelation or the whitening matrix.

*Proof:* Noise decorrelation for the system in Eq. (12) can be accomplished by multiplying both sides of Eq. (12) by the decorrelation matrix  $\mathbf{D}_k$  as:

$$\begin{aligned} \tilde{\mathbf{r}}_k &= \mathbf{D}_k \mathbf{r}_k \\ &= \sqrt{E_s} \mathbf{D}_k \hat{\mathbf{g}}_k \cdot s_k + \mathbf{D}_k \mathbf{z}_k = \sqrt{E_s} \tilde{\mathbf{g}}_k \cdot s_k + \tilde{\mathbf{z}}_k. \end{aligned} \tag{14}$$

The covariance-matrix of the uncorrelated noise samples  $\tilde{\mathbf{z}}_k = \mathbf{D}_k \mathbf{z}_k$  is as follows:

$$\begin{aligned} \mathbf{R}_k^{\tilde{z}} &= E[\tilde{\mathbf{z}}_k (\tilde{\mathbf{z}}_k)^H] \\ &= E[\mathbf{D}_k \mathbf{z}_k \mathbf{z}_k^H \mathbf{D}_k^H] \\ &= N_0 \left( (\mathbf{R}_k^z)^{-\frac{1}{2}} (\mathbf{R}_k^z)^{\frac{1}{2}} \right) \left( (\mathbf{R}_k^z)^{-\frac{1}{2}} (\mathbf{R}_k^z)^{\frac{1}{2}} \right) = N_0 \mathbf{I}_2 \end{aligned} \tag{15}$$

where  $\mathbf{D}_k = \mathbf{D}_k^H$ ,  $\mathbf{R}_k^z = (\mathbf{R}_k^z)^{\frac{1}{2}} (\mathbf{R}_k^z)^{\frac{1}{2}}$ ,  $(\mathbf{R}_k^z)^{\frac{1}{2}} (\mathbf{R}_k^z)^{-\frac{1}{2}} = (\mathbf{R}_k^z)^{-\frac{1}{2}} (\mathbf{R}_k^z)^{\frac{1}{2}} = \mathbf{I}_2$ , and that completes the proof.

Now, the optimum detection rule for the system in Eq. (13) can be derived by applying the MRC to Eq. (13), i.e. by multiplying both sides of Eq. (13) by  $\tilde{\mathbf{g}}_k^H$  the result can be written as:

$$\alpha_k = \sqrt{E_s} \tilde{\mathbf{g}}_k^H \tilde{\mathbf{g}}_k \cdot s_k + \tilde{\mathbf{g}}_k^H \tilde{\mathbf{z}}_k = \sqrt{E_s} \beta_k \cdot s_k + \tilde{\mathbf{g}}_k^H \tilde{\mathbf{z}}_k, \quad (16)$$

where  $\alpha_k = \tilde{\mathbf{g}}_k^H \tilde{\mathbf{r}}_k$ ,  $\beta_k = \hat{\mathbf{g}}_k^H \mathbf{B}_k \hat{\mathbf{g}}_k$ , and  $\mathbf{B}_k = \mathbf{D}_k^H \mathbf{D}_k = N_0 (\mathbf{R}_k^z)^{-1}$ , thus; the transmitted BPSK symbol from the  $k$ -th CU can be estimated at the DMC as [17]:

$$\hat{s}_k = \arg \min_{s \in \{-1, 1\}} \left\{ \left| \alpha_k - \sqrt{E_s} \beta_k \cdot s \right|^2 \right\} \quad (17)$$

## 2.2. The Error Probability of the Reporting-Channel

The SNR of the received local-decision signal from the  $k$ -th CU at the DMC can be evaluated from Eq. (16) as:

$$\begin{aligned} \gamma_k &= \frac{|\beta_k|^2 E_s}{\mathbb{E}[\tilde{\mathbf{g}}_k^H \tilde{\mathbf{n}}_k (\tilde{\mathbf{g}}_k^H \tilde{\mathbf{n}}_k)^H]} \\ &= \frac{|\beta_k|^2 E_s}{\mathbb{E}[\tilde{\mathbf{g}}_k^H \tilde{\mathbf{n}}_k^H \tilde{\mathbf{n}}_k \tilde{\mathbf{g}}_k]} \\ &= \frac{|\beta_k|^2 E_s}{N_0 \tilde{\mathbf{g}}_k^H \mathbf{I}_2 \tilde{\mathbf{g}}_k} = \frac{\beta_k^2 E_s}{N_0 \beta_k} = \beta_k \cdot \gamma_o \end{aligned} \quad (18)$$

where  $\gamma_o = \frac{E_s}{N_0}$  is the SNR of the reporting-channel without fading.

The conditional symbol-error probability of reporting the  $k$ -th CU local-decision can be found as [17]:

$$e_k / \gamma_k = \frac{1}{\pi} \int_0^{\frac{\pi}{2}} \exp\left(-\gamma_o \frac{\beta_k}{\sin^2 \theta}\right) d\theta \quad (19)$$

The unconditional error probability can be obtained by averaging the conditional error probability in Eq. (19) over the instantaneous signal to noise ratio  $\gamma_o$ . Since  $\beta_k = \hat{\mathbf{g}}_k^H \mathbf{B}_k \hat{\mathbf{g}}_k$  is a quadratic form of the zero-mean complex Gaussian vector of channel vector  $\hat{\mathbf{g}}_k$ , the averaging operation can be performed by finding the characteristic function (CHF) [17, 18] of  $\beta_k$  as:

$$\mathbb{E}\left[e^{(j\omega\beta_k)}\right] = \left[\det\left(\mathbf{I}_2 - j\omega \mathbb{E}[\hat{\mathbf{g}}_k \hat{\mathbf{g}}_k^H] \cdot \mathbf{B}_k\right)\right]^{-1} \quad (20)$$

Using Eq. (19) in Eq. (20) and after a number of algebraic manipulations, the unconditional symbol error probability for reporting the  $k$ -th CU local-decision can be given as [17]:

$$e_k = \frac{1}{\pi} \int_0^{\frac{\pi}{2}} \prod_{l=1}^2 \left[ 1 + \frac{E_b}{N_o} \frac{\delta_l}{\sin^2 \theta} \right]^{-1} d\theta \quad (21)$$

where  $\delta_l$  is the non-zero eigenvalues of  $E[\hat{\mathbf{g}}_k \hat{\mathbf{g}}_k^H] \cdot \mathbf{B}_k$  [18].

### 2.3. Final Decision at the DMC

After recovering all the transmitted local-decisions from the CUs, the DMC employs these decisions to determine the final overall decision according to a decision rule; the decision rule is selected to satisfy specific considerations on the overall false-alarm probability, miss-detection probability or both. Thus, using Eqs. (6) and (7), the overall false-alarm probability and the overall miss-detection probability can be respectively calculated as [9]:

$$O_F = \sum_{d=d_{rule}}^K \binom{K}{d} \tilde{P}_{f_k}^d (1 - \tilde{P}_{f_k})^{K-d} \quad (22)$$

$$O_M = 1 - \sum_{d=d_{rule}}^K \binom{K}{d} (1 - \tilde{P}_{m_k})^d \tilde{P}_{m_k}^{K-d} \quad (23)$$

where  $d_{rule}$ ,  $O_F$ , and  $O_M$  denote the selected decision rule, the overall false-alarm probability, and the overall miss-detection probability, respectively. In literature, the common three decision rules are the AND decision-rule with  $d_{rule}=K$ , the OR decision-rule with  $d_{rule}=1$ , and the majority decision-rule with  $d_{rule}=\lceil K/2 \rceil$ , where  $\lceil b \rceil$  is the ceiling-function that yields the smallest integer which is greater than or equal to the value of  $b$ . Finally, the overall sensing error probability ( $O_s$ ) can be described by [9]:

$$O_s = O_M + O_F \quad (24)$$

Based on the preceding theoretical analyses, Matlab plotted results will be presented in the next section to evaluate the performance of the proposed system.

## 3. RESULTS AND SYSTEM EVALUATION

In this section, plotted results are provided to evaluate the performance of the proposed CSD system. Unless mentioned otherwise, the reduced typical urban (TU) channel model is employed to generate multipath fading channel coefficients.

In Fig. 1, the rank of the noise covariance-matrix  $\mathbf{R}^w$  is plotted as a function of the matrix size for different values of the DMC receiver sampling rates. Fig. 1 illustrates that the noise covariance-matrix  $\mathbf{R}^w$  is a full-rank matrix for the system with DSR receiver. On the other hand, the matrix  $\mathbf{R}^w$  is rank deficient for systems with higher receiver sampling rates. Thus, the inverse of noise covariance-matrix  $\mathbf{R}^w$  exists for systems with DSR receivers; and it can be used to remove the correlation between correlated noise elements, as discussed in the previous section.

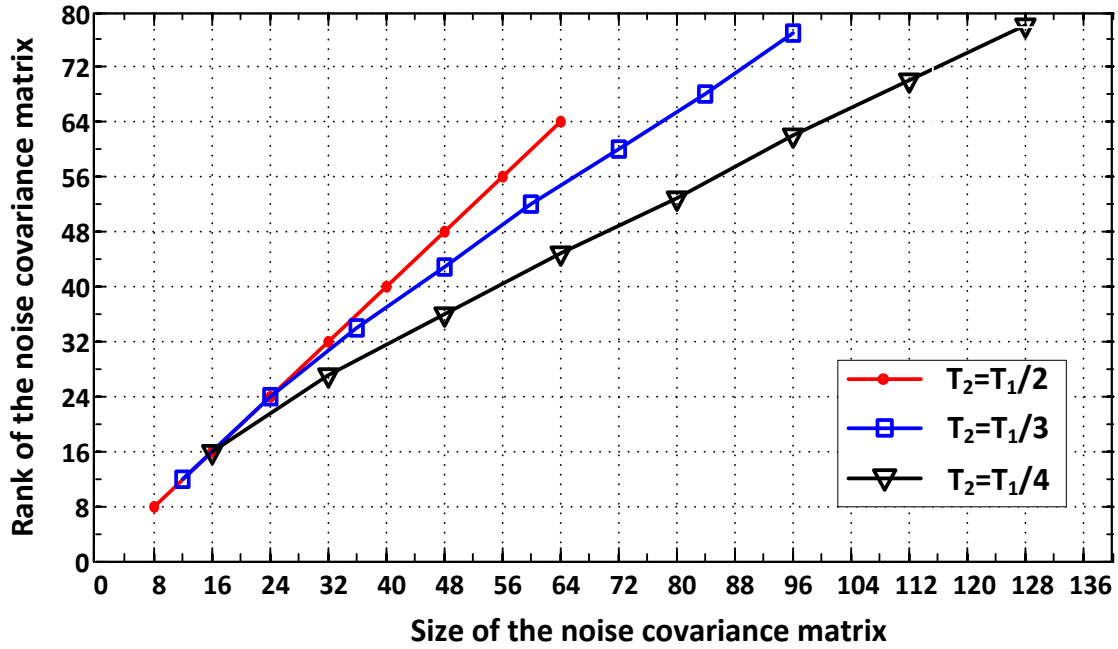


Fig. 1. Rank of the noise covariance-matrix for different DMC receiver sampling rates.

Fig. 2 shows the performance of the CSD system in terms of the DMC receiver operating characteristics' (ROC) curves for various values of  $\gamma_o$ . Here, the sensing-channel SNR is set as  $\gamma_s = 10\text{dB}$ ; the number of CUs is  $K=10$ ; and the AND is used at the DMC as the final-decision rule. It can be observed from the figure that the detection performance of the CSD system can be enhanced by  $\gamma_o$  increase. Also, CSD system with DSR DMC receiver shows an apparent performance improvement over an equivalent conventional CSD system with  $T_2 = T_1$ .

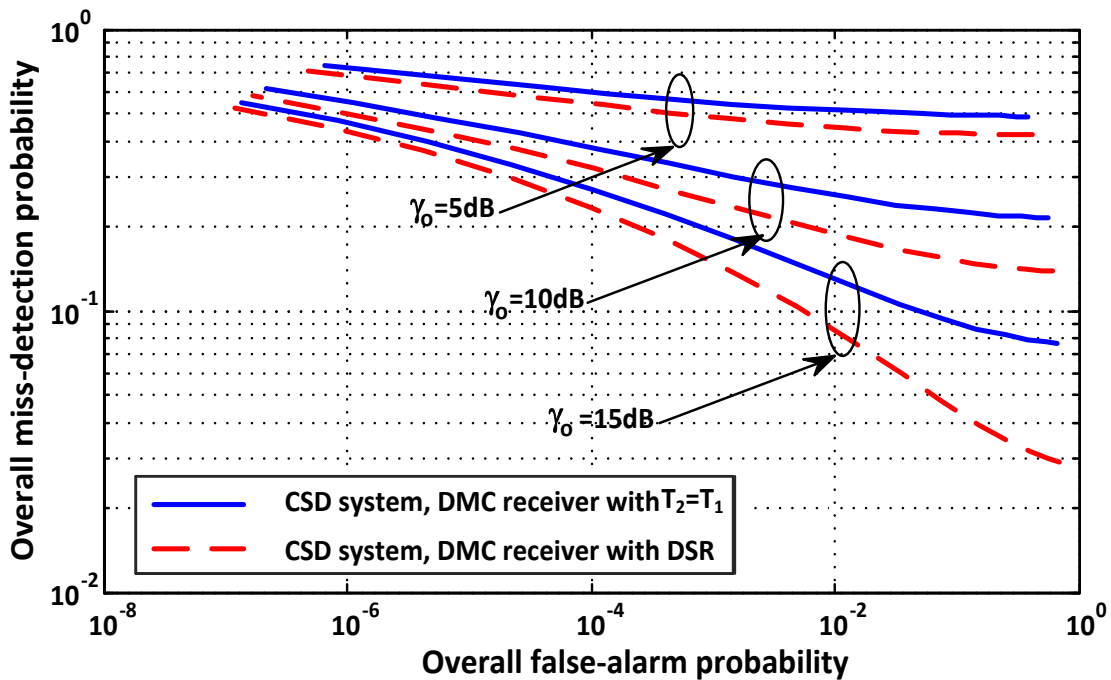


Fig. 2. The receiver operating characteristics' curves for different values of  $\gamma_o$ .

For example, at  $\gamma_o = 10\text{dB}$  and an overall false-alarm probability of  $10^{-2}$ , the overall miss-detection probabilities are 0.19 and 0.275 for the proposed system with DSR and the conventional system with  $T_2 = T_1$ , respectively. That means a nearly 31% decrease in the overall miss-detection probability can be achieved by the proposed system compared to the conventional system; moreover, the reduction percentage increases to 43.3% at  $\gamma_o = 15\text{dB}$ . The performance enhancement of CSD systems with DSR DMC receiver is mainly due to the multipath diversity collected at the DMC receiver.

The effect of timing-phase offset  $\tau$  between the CU transmitter and the DMC receiver on the overall sensing error probability of CSD systems with DSR DMC receiver is illustrated in Fig. 3.

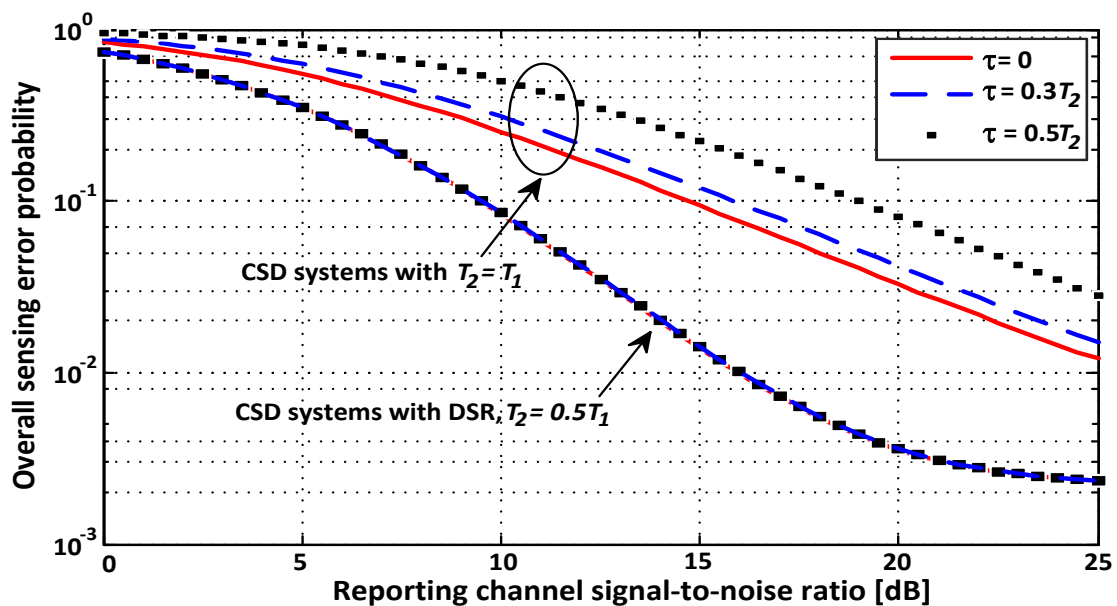


Fig. 3. The overall sensing error probability versus  $\gamma_o$  for different values of timing-phase offset.

For comparison purposes, the overall sensing error probability versus  $\gamma_o$  are also shown for CSD systems with  $T_2 = T_1$ . In this figure, the OR decision rule,  $K=10$ ,  $\gamma_s = 15\text{ dB}$ , and  $\lambda = 50$  is considered for all systems. Due to the multipath diversity, a significant performance improvement of CSD systems with DSR receiver at the DMC over equivalent conventional CSD systems with  $T_2 = T_1$  is achieved as shown in the figure. At an overall sensing error probability of  $10^{-1}$ , systems with DSR DMC receivers outperform conventional systems by about 5.5 dB, 6.5 dB, and 9.5 dB for  $\tau=0$ ,  $\tau= 0.3T_1$ , and  $\tau= 0.5T_1$  respectively. That is, more transmission energy is needed in the conventional system with  $T_2 = T_1$  to reach the same overall sensing error probability as in the proposed system. Also, the figure shows that the timing-phase offset has no effect on the sensing error probability of the CSD systems with DSR DMC receiver while it degrades the overall sensing error probability of equivalent CSD systems with  $T_2 = T_1$ .

The ROC performance curves at the DMC for CSD systems at two different sampling rates and various values of timing-phase offset, where the majority rule,

$K=10$ ,  $\gamma_s=10$  dB, and  $\gamma_o=10$  dB used for all systems, are shown in Fig. 4. Also, the ROC curves for the CSD systems with  $T_2 = T_1$  and a noise-free reporting-channel are plotted in the same figure. The following notes can be made about Fig. 4. First, at the same overall false alarm probability, the overall miss-detection probability increases with the timing-offset increase for CSD systems with  $T_2 = T_1$ , while the timing offset does not affect CSD systems with DSR DMC receiver. Second, at a certain overall false alarm probability, systems with DSR DMC receiver have a smaller overall miss-detection probability compared to CSD systems with a conventional DMC receiver.

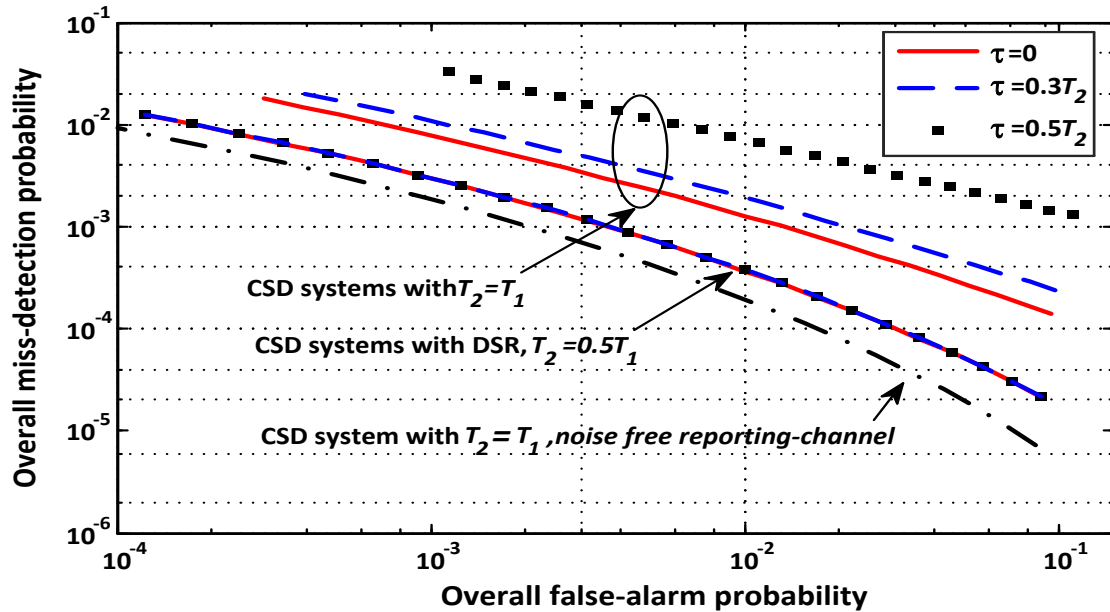


Fig. 4. The ROC performance of systems with DSR DMC receivers at different values of  $\tau$ .

For example, at an overall false-alarm probability of  $10^{-2}$  and  $\tau=0$ , the overall miss-detection probability of the proposed system is 0.0004 while the overall miss-detection probability of the conventional system with  $T_2 = T_1$  is 0.0015. This means that employing DSR at the DMC receiver reduces the overall-miss detection probability by 73.3% compared to a similar system with  $T_2 = T_1$ . The reduction percentage becomes 80% and 94.2% at  $\tau=0.3T_1$  and  $\tau=0.5T_1$ , respectively. Finally, compared to a noise-free system, the performance of the CSD system with DSR DMC receiver outperforms a similar system but with  $T_2 = T_1$ .

The impact of the  $\gamma_o$  on the overall false-alarm probability for CSD systems with DSR DMC receiver is presented in Fig. 5, which is plotted using: the OR decision rule,  $\gamma_s=10$  dB, and  $K=10$ . Results are obtained at  $\gamma_o=5$  dB,  $\gamma_o=10$  dB, and  $\gamma_o=15$  dB, respectively. At a specific threshold value, the overall false-alarm probability decreases with an increase in  $\gamma_o$ . Also, as expected, the proposed system with DSR DMC receiver shows performance improvements over equivalent CSD systems but with a sampling period of  $T_2 = T_1$  at the DMC receiver. For example, at  $\lambda=55$  and  $\gamma_o=5$  dB; a 20% reduction in the overall false-alarm probability of the proposed CSD system with DSR DMC receiver is achieved compared to a similar system but with  $T_2=T_1$ . Furthermore,

the reduction percentage jumps to 29% and 63.33% at  $\gamma_o = 10\text{dB}$  and  $\gamma_o = 15\text{dB}$ , respectively.

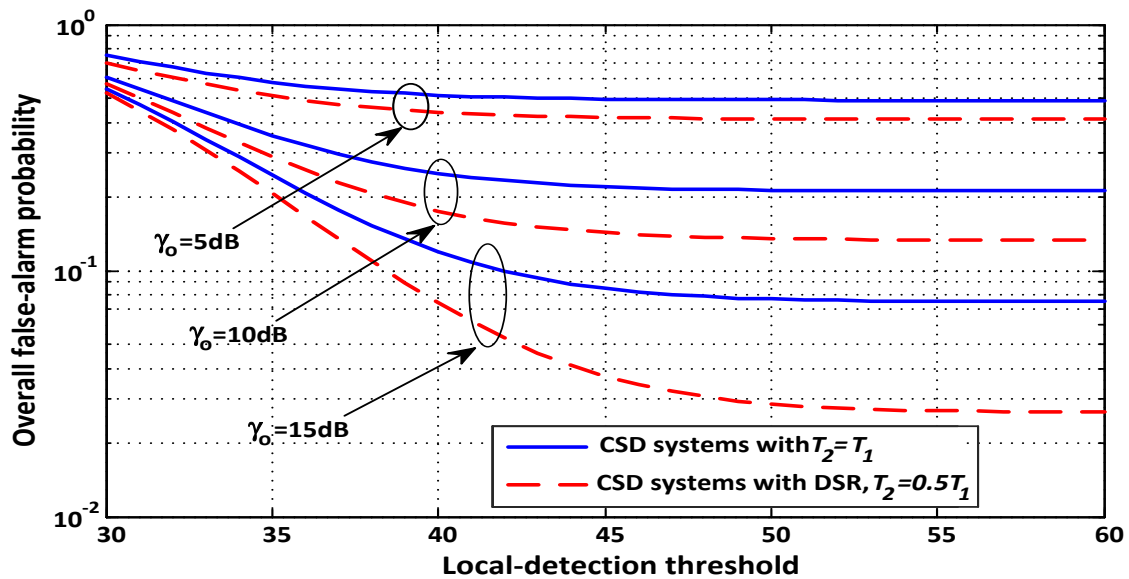


Fig. 5. The overall false-alarm probability versus threshold for different values of  $\gamma_o$ .

The overall sensing error probabilities of the CSD system with a majority decision rule under different system parameters are shown in Fig. 6, where  $K=8$ , and  $\gamma_o = 5\text{ dB}$  are used for all systems. As expected, any increase in  $\gamma_s$  leads to an overall sensing improvement. The performance of the CSD system with DSR DMC receiver outperforms the conventional CSD system with  $T_2=T_1$ . As an illustration, at  $\lambda = 25$  and  $\gamma_s = 10\text{dB}$  the overall sensing error probability is 0.0375 for the conventional system while it decreases to about 0.012 for the proposed system; this is equivalent to a 68% reduction in the overall sensing error probability of the proposed CSD system compared to the conventional system.

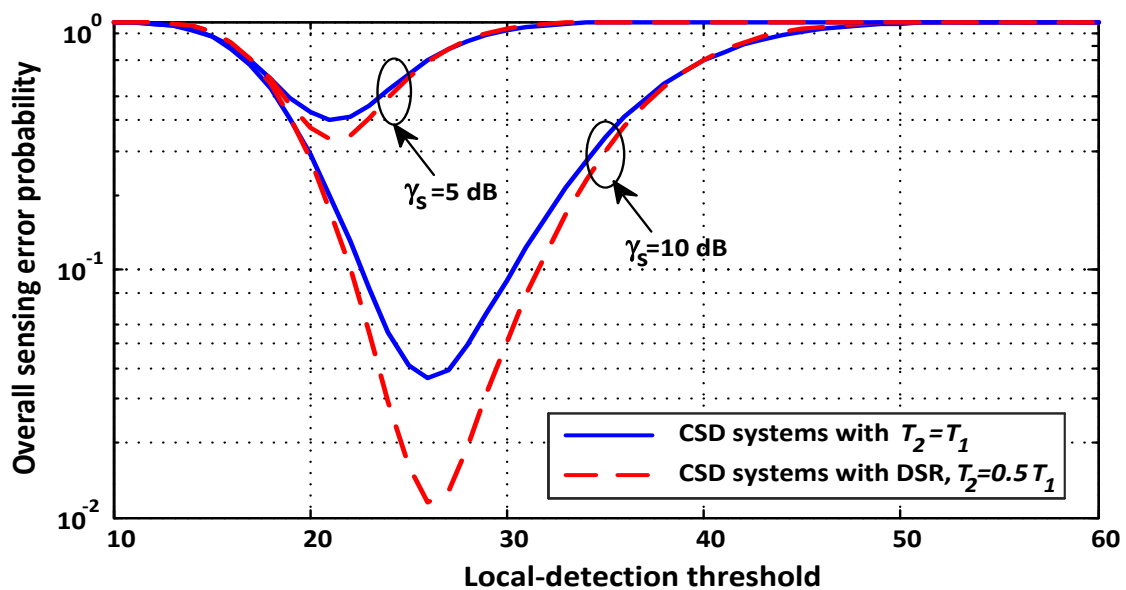


Fig. 6. The overall sensing error probability versus threshold ( $\lambda$ ) for two different values of  $\gamma_s$ .

Fig. 7 compares the overall sensing error probability of CSD systems at two different DMC sampling rates and for three decision rules. A considerable performance improvement of the proposed CSD systems over similar CSD systems but with  $T_2 = T_1$  is shown in the figure. The performance improvement is mainly due to the introduced multipath diversity collected at the DMC receiver.

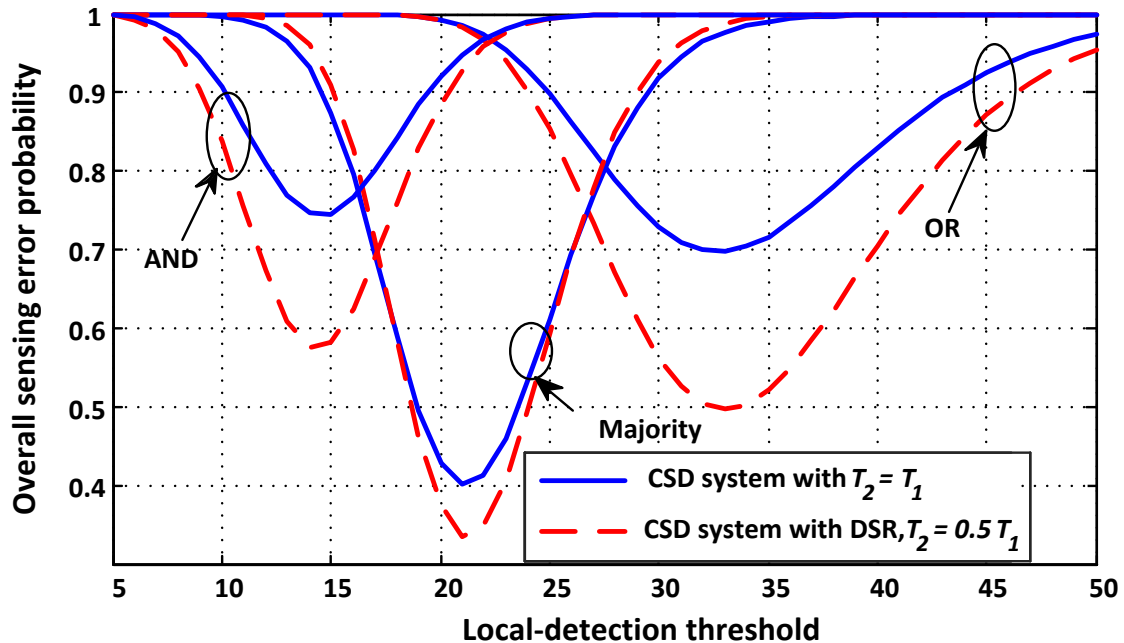


Fig. 7. The overall sensing error probability as a function of  $\lambda$  for three different decision rules where the number of CUs is  $K=8$ ,  $\gamma_s=10$  dB and  $\gamma_o=10$  dB.

Compared to the conventional CSD system with  $T_2 = T_1$ , the minimum value of the overall sensing error probability for the CSD system with DSR DMC is reduced by 23.33%, 17.5%, and 28.6% for AND, majority, and OR, respectively. It can be easily seen that the majority decision rule shows the best overall sensing error probability for both the proposed and conventional CSD systems. Under the same system configurations, the optimum threshold is the highest at the OR decision rule while it is the minimum at the AND decision rule.

Fig. 8 shows the overall false-alarm probability at the DMC for the proposed system with DSR DMC receiver, and the conventional system with  $T_2 = T_1$ . The length of channel impulse response for the reporting channel is set as  $L=4$  whereas the overall detection probability is set as  $O_d = 1 - O_m = 0.9$ . In [16, Fig. 3], four fusion approaches for cooperative spectrum detection are shown. These approaches are: decision combination with OR, soft fusion, fusion with channel statistics, and fusion using perfect CSI [16]. Both Fig. 8 and [16, Fig. 3] were obtained with  $K=8$ ,  $L=4$ ,  $O_d=0.9$ , and  $\gamma_o=4$  dB. By comparing the two figures, the following observations can be made: First, at  $\gamma_o=4$  dB, the proposed CSD system with DSR receiver has a better performance than a system with the decision combination approach; however the CSD system has a comparable performance to a cooperative system with soft fusion. Second, the

reporting channel SNR greater than 10 dB, the performance of the proposed system with DSR outperforms both decision combination and soft fusion approaches while it has a similar performance to fusion with channel statistics and fusion using perfect CSI.

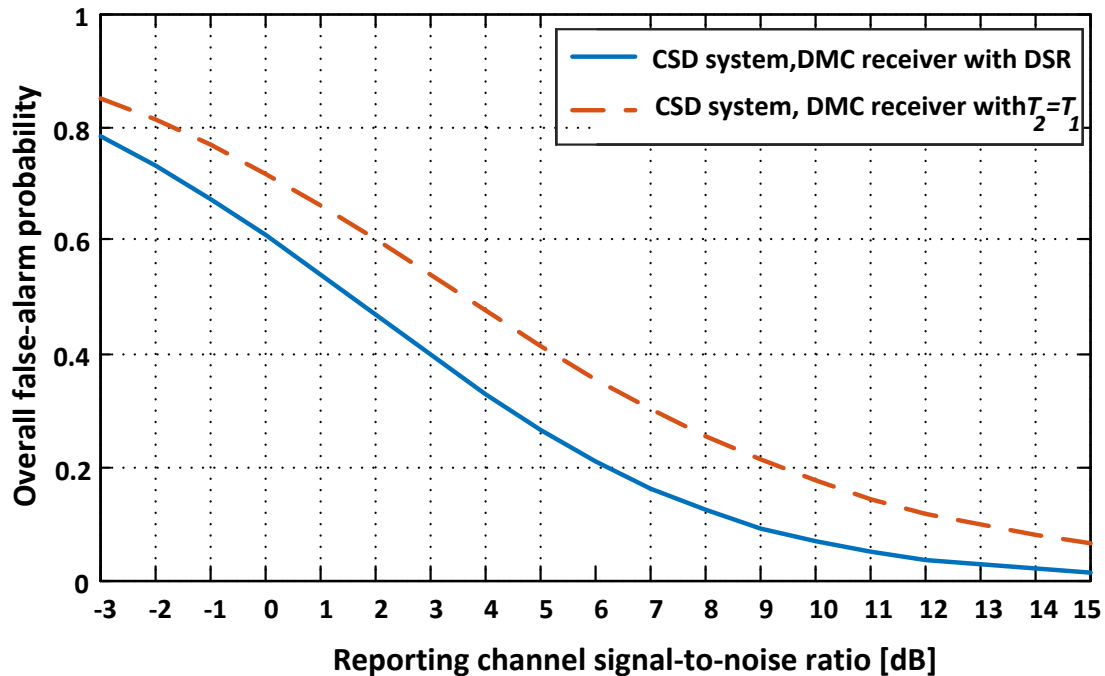


Fig. 8. The overall false-alarm probability as a function of reporting channel signal-to-noise ratio.

#### 4. CONCLUSION

A double-sampling multicarrier CSD system has been introduced in this paper. The results show that the DSR employed by the receiver at the DMC introduces multipath diversity, which in turn reduces the errors of reporting local decisions from CUs to the DMC. The reduction in the reporting errors enhances the performance of the CSD. Also, compared to equivalent CSD systems, the proposed CSD system with DSR is robust against the timing phase-offset between the transmitter at the CU and the receiver at the DMC. Moreover, all the advantages of using DSR in cooperative spectrum sensing were achieved without introducing any modifications to CUs.

#### REFERENCES

- [1] J. Mitola, G. Maguire, "Cognitive radio: Making software radios more personal," *IEEE Personal Communications*, vol. 6, no. 4, pp. 13 - 18, 1999.
- [2] G. Padmavathi, S. Shanmugavel, "Performance analysis of cooperative spectrum sensing technique for low SNR regime over fading channels for cognitive radio networks," *Indian Journal of Science and Technology*, vol. 8, no. 16, 2015.
- [3] S. Atapattu, C. Tellambura, H. Jiang, *Energy Detection for Spectrum Sensing in Cognitive Radio*, New York, NY: Springer New York, 2014.
- [4] I. Akyildiz, B. Lo, R. Balakrishnan, "Cooperative spectrum sensing in cognitive radio networks: a survey," *Physical Communications*, vol. 4, no. 1, pp. 40-62, 2011.

- [5] K. Letaief, W. Zhang, "Cooperative communications for cognitive radio networks," *Proceedings of the IEEE*, vol. 97, no. 5, pp. 878–893, 2009.
- [6] T. Aysal, S. Kandeepan, R. Piesiewicz, "Cooperative spectrum sensing over imperfect channels," *2008 IEEE Globecom Workshops*, pp. 1-5, 2008.
- [7] T. Aysal, S. Kandeepan, R. Piesiewicz, "Cooperative spectrum sensing with noisy hard decision transmissions," *2009 IEEE International Conference on Communications*, pp. 1-5, 2009.
- [8] Z. Wang, D. Wei, Z. Chen, "Cooperative spectrum sensing over imperfect reporting channels in cognitive radio for Wi-Fi networks," *2013 3rd International Conference on Consumer Electronics, Communications and Networks*, pp. 203-208, 2013.
- [9] B. Selim, O. Alhussein, G. Karagiannidis, S. Muhaidat, "Optimal cooperative spectrum sensing over composite fading channels," *2015 IEEE International Conference on Communication Workshop*, pp. 520-525, 2015.
- [10] D. Bera, I. Chakrabarti, S. Pathak, "Modelling of cooperative spectrum sensing over rayleigh fading without CSI in cognitive radio networks," *Wireless Personal Communications*, vol. 86, no. 3, pp. 1281–1297, 2015.
- [11] A. Kortun, T. Ratnarajah, M. Sellathurai, C. Zhong, C. Papadias, "On the performance of eigenvalue-based cooperative spectrum sensing for cognitive radio," *IEEE Journal of Selected Topics in Signal Processing*, vol. 5, no. 1, pp. 49–55, 2011.
- [12] G. Ganesan, Y. Li, "Cooperative spectrum sensing in cognitive radio, part I: two user networks," *IEEE Transactions on Wireless Communications*, vol. 6, no. 6, pp. 2204–2213, 2007.
- [13] J. Lunden, V. Koivunen, A. Huttunen, H. Poor, "Collaborative cyclostationary spectrum sensing for cognitive radio systems," *IEEE Transactions on Signal Processing*, vol. 57, no. 11, pp. 4182–4195, 2009.
- [14] G. Kumar, M. Gajula, S. Nallagonda, "Cooperative spectrum sensing in log-normal shadowing environment with erroneous sensing and reporting channels," *2018 Second International Conference on Advances in Electronics, Computers and Communications*, pp. 1-6, 2018.
- [15] H. Huang, C. Yuan, "Cooperative spectrum sensing over generalized fading channels based on energy detection," *China Communications*, vol. 15, no. 5, pp. 128–137, 2018.
- [16] R. Xu, M. Chen, J. Zhang, H. Wang, W. Yu, "Report the sensing results using OFDMA in cooperative spectrum sensing," *2010 International Conference on Wireless Communications and Signal Processing*, pp. 1-6, 2010.
- [17] J. Wu, "Proportionally sampled multicarrier modulation," *2008 IEEE International Conference on Communications*, pp. 4845-4849, 2008.
- [18] J. Wu, Y. Zheng, "Oversampled orthogonal frequency division multiplexing in doubly selective fading channels," *IEEE Transactions on Communications*, vol. 59, no. 3, pp. 815–822, 2011.